Topologically protected strong photon-exciton coupling

Zhiyuan Qian,[1] Ye Chen,[1] and Chao Peng[1,2,*]

[1]*State Key Laboratory of Advanced Optical Communication Systems and Networks, Department of Electronics & Frontiers Science Center for Nano-optoelectronics, Peking University, Beijing 100871, China*

[2]*Peng Cheng Laboratory, Shenzhen 518055, China*

(Received 21 June 2023; accepted 22 September 2023; published 10 October 2023)

We propose that strong photon-exciton coupling performed by a plasmonic nanoantenna and a single emitter can be protected in the well-designed topological photonic structure as an environment. Topological robustness leads to a reduction of metal loss, which makes Rabi splitting much larger. The strong coupling regime gets more stable in the topological systems because the sensitivity characterized by Rabi splitting can always remain small compared to the sensitive nontopological systems. Moreover, we show that the Rabi splitting under topological protection is immune to defects or impurities that can destroy strong coupling in nontopological systems. This topologically protected strong coupling mechanism offers more improvement in the applications of on-chip quantum integration, single quantum sources, and quantum information processing.

DOI: 10.1103/PhysRevA.108.043706

I. INTRODUCTION

Cavity quantum electrodynamics (CQED) has been a rapidly growing field because of the urgent requirement for on-chip quantum information and scalable quantum network [1–6]. By providing an ultrasmall optical mode volume to enhance light-matter interaction, plasmonic devices are suitable platforms to reach strong coupling [7–9]. In contrast to cold atom studies [10–12], the strong coupling can be achieved at room temperature by constructing gap surface plasmon structures [13–15] or fabricating special emitters like *J* aggregates [16,17], Rhodamine 6G molecules [18], and quantum dots [19]. These quantum plasmonic devices promise an essential impact on the fundamental physics of surface plasmons and open up a new way in the applications of single-photon sources [20,21], quantum nodes [1,22], and quantum gates [23,24]. In recent years, it has been noticed that Rabi splitting is quite sensitive to environmental permittivity leading to the development of quantum plasmon sensing based on strong coupling [25,26]. However, applications such as single-photon sources, on-chip integration devices, and quantum information processing require stable Rabi splitting, which the embedding environment only affects a little.

The concept of topology has been widely used in micro and nanophotonics [27–30]. Topological optical states, including edge states [31,32], interface states [33,34], corner states [35,36], and bound states in the continuum (BIC) [37,38] are described by topological invariants in the reciprocal space. Various nanophotonic designs are proposed to realize and utilize the topological features, such as Su-Schrieffer-Heeger (SSH) models [39–41], honeycomb photonic crystals [31,32], coupled-resonator optical waveguides (CROW) [42,43], and BIC photonic crystal slabs [44,45]. These structures exhibit immunity to a broad class of impurities and defects, i.e., topological protection or robustness, which is utilized to fabricate plenty of nanophotonic structures, like topological sources of quantum light [46], topological lasers [47], and topological waveguides [48]. Recently, topological protection has been introduced into the Purcell enhancement under topological protection to overcome the scattering and absorption in nano-CQED systems [49]. However, the photonic research of strong-coupling-combined topological features has yet to be achieved. Since topological structures can efficiently protect some quantum states and effects [46,50,51], revealing the behavior of strong photon-exciton coupling is meaningful under topological protection.

In this paper, we find that topological structures can protect strong coupling regimes by carefully designing a resonant nanoantenna embedded in a one-dimensional (1D) topological photonic structure [Fig. 1(a)]. The topological structure is much larger than the strong coupling system consisting of a silver nanoantenna and a single emitter, which means it can be treated as a dielectric environment. The topological environment reduces cavity loss from metal nanoantenna, so the Rabi splitting in topological structures is more significant than in nontopological structures. Rabi splitting can be immune to the perturbation of environmental permittivity under topological protection, even if the changes are large enough to destroy the strong coupling regime in the nontopological systems. Thus, topological photonic structures can efficiently protect the strong coupling regime and significantly reduce the difficulty of reaching strong coupling. Our work applies topological protection to the strong coupling regime of the CQED system in which more tunable parameters are involved than the weak coupling regime [49], which is of great help for the applications of on-chip integrated quantum devices, single photon sources, and quantum information processing.

II. MODULE SETUP OF STRONG COUPLING UNDER TOPOLOGICAL PROTECTION

To investigate the strong coupling under topological protection, we set up a 1D topological photonic crystal (PC)

*pengchao@pku.edu.cn

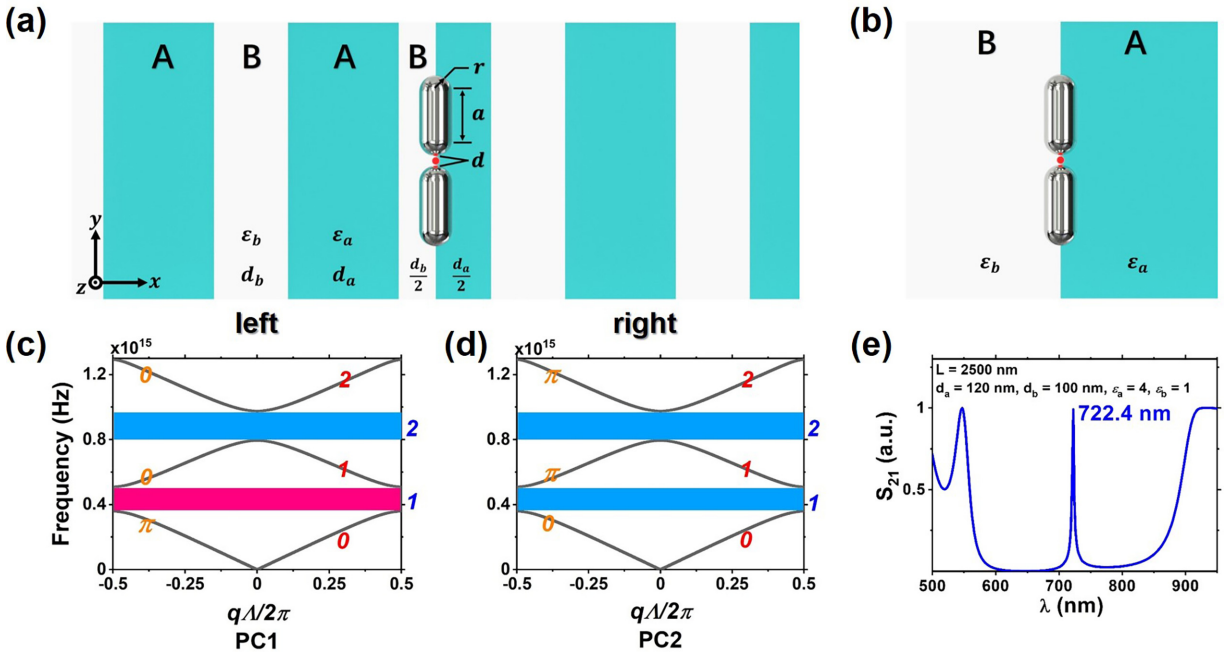

FIG. 1. (a) Schematic diagram of the 1D topological structure composed of a 1D topological PC with the left and right semi-infinite PCs, a resonant silver nanoantenna, and a single emitter. (b) Schematic diagram of the nontopological strong coupling system consisting of the same nanoantenna and emitter as (a). The band-gap structures of (c) left and (d) right semi-infinite PC with Zak phases marked in orange numbers and topological numbers marked in blue (<0) or pink (>0) strip. (e) The transmission spectrum of 1D topological PC showing the edge state at $\lambda = 722.4$ nm. Layers A and B parameters are $\varepsilon_a = 4$, $d_a = 120$ nm, and $\varepsilon_b = 1$, $d_b = 100$ nm, respectively.

containing a resonant plasmonic nanoantenna and a single emitter [Fig. 1(a)]. The control group module is also constructed through the same structure of nanoantenna and emitter in the nontopological structure consisting of two semi-infinite spaces [Fig. 1(b)]. The nanoantenna is comprised of two silver nanorods, and the single emitter is at the center of the gap between nanorods. The nanogap structure can work as an open nanocavity [49,52,53]. In the nanogap plasmonic structures, ultrasmall spatial volume and gap surface plasmon result in ultrasmall optical mode volume, which enhances strong photon-exciton coupling [54–56]. Thus, the entire system reaches the strong coupling regime.

A 1D topological PC surrounding the strong coupling systems comprises two semi-infinite PC with layers A and B. The edge state of the topological structure originates from the Zak phase and topological numbers of energy band-gap structure [Figs. 1(c) to 1(e)], depending on the permittivity and size of dielectric layers [33,34]. Plenty of works studied the topological protection given by the edge state [27–30,47,57–60]. It also has been proven that this kind of edge state is robust to small plasmon nanoparticles and the perturbation of unit cells [49], allowing nanoantenna embedded in the topological PC without influence on the edge state. Thus in our module, the 1D topological PC provides the outer stable dielectric environment for strong coupling systems, so the strong coupling under topological protection can be explored.

The interaction between the quantized field and quantum emitter in the field of CQED is usually described as a Jaynes-Cummings model with a single-mode cavity and a two-level emitter [61,62]. Under the dipole and rotating wave approximations, the Hamiltonian and master equation [10,12,63,64] of CQED systems can be written as $H = \hbar\omega_a\sigma^\dagger\sigma + \hbar\omega_c a^\dagger a + \hbar g(\sigma^\dagger a + \sigma a^\dagger)$ and $\dot{\rho} = -(i/\hbar)[H,\rho] - (\gamma/2)(\sigma^\dagger\sigma\rho - \sigma\rho\sigma^\dagger + \text{H.c.}) - (\kappa/2)(a^\dagger a\rho - a\rho a^\dagger + \text{H.c.})$, where ω_a and ω_c are the frequencies of the emitter and resonant nanocavity, respectively, $\sigma^\dagger$ (σ) is the rising (lowering) operator of the emitter, and $a^\dagger$ (a) is the rising (lowering) operator of the nanocavity. The most important parameters of CQED systems are g, κ, and γ. g denotes the coupling coefficient between the emitter and cavity mode, which can be obtained [55,65] as $g = \vec{E}\cdot\vec{\mu}/\hbar$, where $\vec{E}$ is the electric field corresponding to a single excitation of the nanocavity and $\vec{\mu}$ is the dipole moment of the emitter. κ describes the dissipative channel from the nanocavity to the thermal reservoir via Ohmic loss, which can be obtained by the full width at half maximum (FWHM) of the absorption spectrum of the nanocavity. γ describes the dissipative channel from the emitter to modes other than the nanocavity mode. Note that, in this work, the nanocavity modes are provided by silver nanoantenna, not the photonic crystal. Considering a strong coupling system under topological protection, the topology will reduce the cavity loss, i.e., κ, which will be explained later.

To compute the parameters of strong coupling systems in the topological structure, three-dimensional (3D) finite-element simulations are performed using commercial COMSOL MULTIPHYSICS software, which can simulate optical modes, photon propagation, and photon-emitter coupling for various photonic structures [25,49,55,66,67]. After obtaining the parameters g, κ, γ combining with frequencies ω_a and ω_c, one can figure out the fluorescence spectra and dynamical evolution via the PYTHON TOOLBOX QUTIP [68] based on

the Hamiltonian and master equation. The fluorescence spectrum can be written as $S(\vec{r},\omega) = \mathrm{Re}[\int d\tau \langle E^-(\vec{r},t)E^+(\vec{r},t+\tau)\rangle \exp(i\omega t)]/\pi$, which is the Fourier-transformed electric field operator $\langle E^-(\vec{r},t)E^+(\vec{r},t+\tau)\rangle \propto \langle \sigma^\dagger(t)\sigma(t+\tau)\rangle$. The Rabi splitting energy E^R is the difference between two peaks in the fluorescence spectra. The Zak phase and topological number of the outer 1D topological PC can be calculated through the band-gap structure, which was clarified in the previous works [33,49].

As shown in Fig. 1(a), the 1D topological PC is made up of two kinds of layers A and B with the thickness of $d_a = 120\,\mathrm{nm}$ and $d_b = 100\,\mathrm{nm}$, and the permittivity of $\varepsilon_a = 4$ and $\varepsilon_b = 1$, respectively. According to the band-gap structure [Figs. 1(c) and 1(d)], the different Zak phase distributions bring the opposite topological numbers in both sides of the PC at the first gap, implying the existence of the edge state, which is determined at $\lambda = 722.4\,\mathrm{nm}$ by the transmission spectrum [Fig. 1(e)]. To simulate the infinite 1D topological PC, as shown in Fig. 1(a), the boundaries parallel to the yz plane are under the scattered boundary condition, while the boundaries parallel to the x axis are under the periodic condition so that the influence of the size limit of side length L in the yz plane can be neglected. It was proved that $L = 2500\,\mathrm{nm}$ and five periods for both semi-infinite PC sizes are enough to act as a 1D infinite PC in the propagation direction of the x axis [49]. The inside silver nanoantenna is placed parallel to the interface of two semi-infinite PCs and divided into two equal parts, with the resonant wavelength at 722.4 nm and the gap distance $d = 5\,\mathrm{nm}$. The two nanorods' radius r can range from 3 to 10 nm, and the resonance length follows the radius to keep the resonant wavelength of the entire nanoantenna unchanged. The dielectric constant of silver is taken from the experimental data [69]. A point source with a y-polarized dipole is placed in the middle of the gap structure as the single emitter. The electric current dipole moment is $p = 10^{-12}\,\mathrm{Am}$ and the dipole moment $\mu = 0.2\,\mathrm{enm}$.

As shown in Fig. 1(b), the control group module uses two semi-infinite free spaces with $\varepsilon_a = 4$ and $\varepsilon_b = 1$ instead of the topological structure to perform the nontopological environment. The entire space volume and boundary conditions of the nontopological case are the same as those of the topological case. The silver nanoantenna is placed parallel to the interface of two semi-infinite spaces and divided into two equal parts with the same resonant wavelength, gap distance, and size as that of the topological case. Therefore, we can compare strong coupling behavior with or without topological structure.

III. INFLUENCE OF TOPOLOGY ON RABI SPLITTING WITH DIFFERENT SIZES OF CAVITIES

The parameters of strong coupling with and without topological structure are given in Fig. 2(a). With the nanoantenna's size increment, the coupling coefficient g decreases slowly while the cavity loss κ rises. The spontaneous emission rate γ ranges from 2 to 4 meV, which is relatively weak compared with g and κ. Rabi splitting [12,25,63] can be described as $E^R = \sqrt{4g^2 - (\kappa-\gamma)^2/4}$, therefore, Rabi splitting mainly depends on g and κ changing by the size of the nanoantenna. When g rises and κ reduces with a smaller nanoantenna size, Rabi splitting energy E^R gets larger. Thus the Rabi splitting energy E^R grows with the smaller nanoantenna size because of the stronger light confinement [Figs. 2(b) and 2(c)].

The overlap between the topological state and localized surface plasmon determines how much topological states reduce the metal loss of the nanocavity. If the near-field overlapping is sufficiently strong, like the case shown in Fig. 1(a), it can cause topological states to reshape the field distribution of the surface plasmon and lower its localization, meaning reduced metal loss [49], so κ_{topo} in the topological structure is smaller than κ_{notopo} of the nontopological structure [Fig. 2(a)], where the subscripts "topo" and "notopo" represent the topological and nontopological cases, respectively. Meanwhile, topology cannot interfere with the energy exchange between the emitter and nanocavity, so g_{topo} and g_{notopo} are almost the same shown in Fig. 2(a). Similarly, the topology cannot affect the spontaneous emission directly, so γ_{topo} and γ_{notopo} are also nearly the same [Fig. 2(a)]. Therefore, it is worth stressing that the topological PC can enhance the Rabi splitting energy E^R rather than a nontopological dielectric environment due to less cavity loss. According to Figs. 2(b) and 2(c), the fluorescence spectra in the topological structure have similar changing trends with those in nontopological construction, but the patterns of the topological case are more expanded. For example, when the nanoantenna has the parameters of $r = 6.5\,\mathrm{nm}$, $a = 21.45\,\mathrm{nm}$, and $d = 5\,\mathrm{nm}$, Rabi splitting E^R is 27.02 meV for the topological structure and 21.18 meV for the nontopological environment [Fig. 2(d)], which makes it clear to find that the E^R in the topological structure is larger than that in the nontopological environment. To observe the enhancement of Rabi splitting more clearly, we give the comparison of Rabi splitting energy between topological and nontopological cases, i.e., E^R_{topo} and E^R_{notopo}, shown in the orange and dark yellow lines of Fig. 2(a), respectively. When the nanoantenna is very small such as $r = 3\,\mathrm{nm}$, E^R_{topo} and E^R_{notopo} seems the same, while the Rabi splitting difference $E^R_{\mathrm{topo}} - E^R_{\mathrm{notopo}}$ grows rapidly with the increment of the nanoantenna's size.

In particular, the topology mechanism not only enhances the Rabi splitting, but also protects the strong coupling regime from being destroyed by the large cavity size. In our module, as shown in Figs. 2(a), 2(c) and 2(e), when the nanoantenna's radius is $r \geqslant 8\,\mathrm{nm}$, the Rabi splitting disappears in the nontopological structure, which means too large a nanoantenna breaks the condition of strong coupling because κ_{notopo} grows much larger than g_{notopo} [Fig. 2(a)]. Meanwhile, as shown in Figs. 2(a), 2(b) and 2(d), Rabi splitting remains in the topological case due to the smaller κ_{topo} [Fig. 2(a)], thus strong coupling still exists. Therefore, topological robustness reduces the metal loss of the nanocavity, which enhances the Rabi splitting and protects the strong coupling regime from being destroyed by the large cavity size.

IV. TOPOLOGICALLY PROTECTED STRONG COUPLING AGAINST DEFECTS AND IMPURITIES

In general, strong coupling systems are susceptible to the variation of environmental permittivity in the nontopological environment [25,26]. When considering the surrounding topological dielectric environment, the behavior of nanoscale

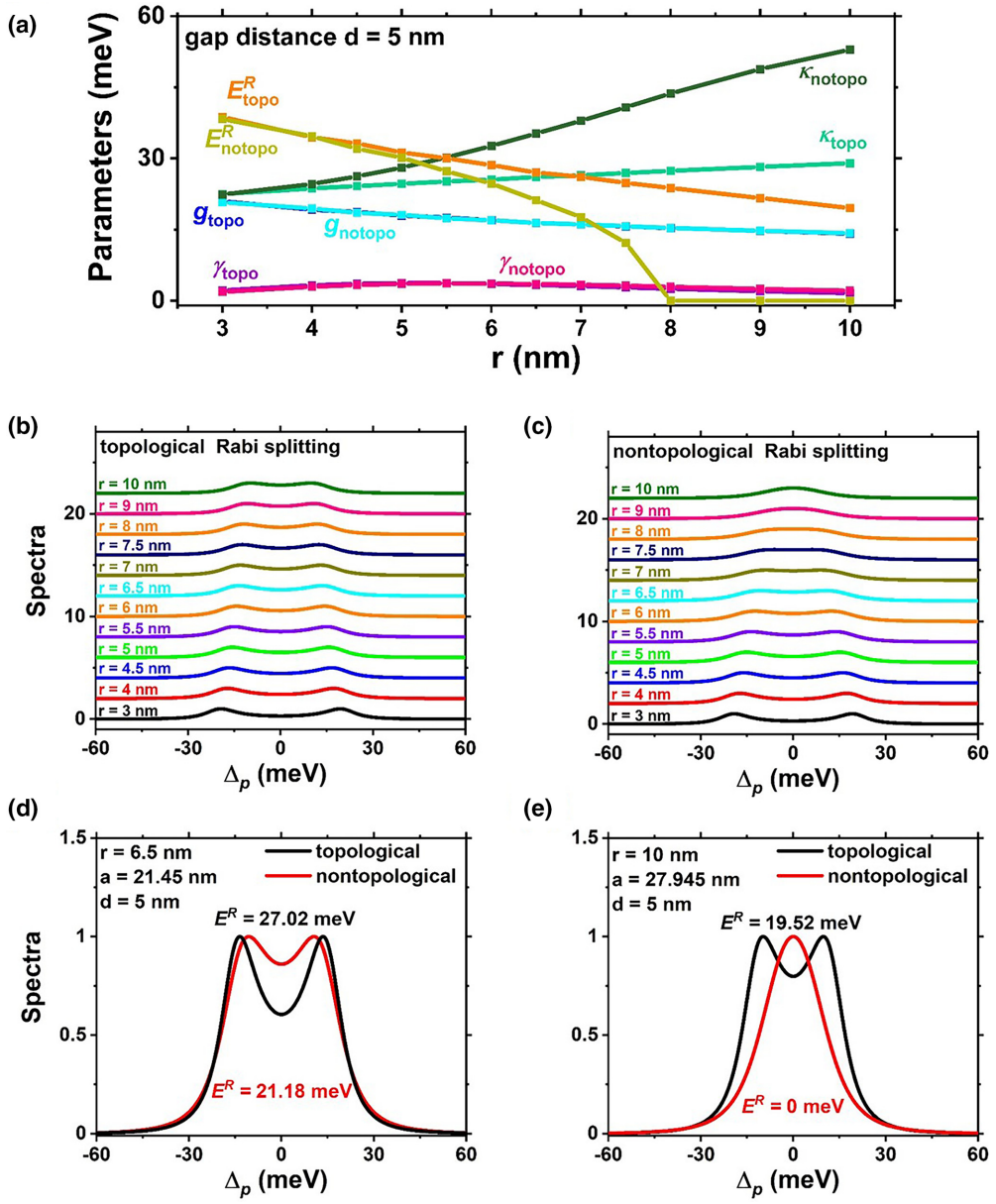

FIG. 2. The behavior of strong coupling systems with and without topological structure. (a) Coefficients g, κ, γ and Rabi splitting energy E^R with and without topological structure, as a function of nanoantenna's radius r. Rabi splitting for different sizes of nanoantenna (b) with or (c) without topological protection, as a function of probe detuning $\Delta_p = \omega_p - \omega_c$. Rabi splitting with and without topological structure with the parameters of nanoantenna (d) $r = 6.5$ nm, $a = 21.45$ nm, $d = 5$ nm, and (e) $r = 10$ nm, $a = 27.945$ nm, $d = 5$ nm, as a function of Δ_p.

strong coupling systems is quite different. The gap surface plasmon of the silver nanoantenna can be seen as a defect mode within a 1D topological PC with no influence on the edge state [49]. Still, it can also be topologically protected, and a similar topological protection of the photonic midgap defect modes was proved recently [70]. When the outside dielectric changes, strong coupling systems lose their sensitivity and become immune to the defects and impurities of the environment. Here we design several situations of defects and impurities based on environmental changes to perform the characteristic of topological protection of strong coupling.

We use the definition of sensitivity based on Rabi splitting E^R to quantify the influence of strong coupling by the environment [25], which is $S = |\Delta E^R|/|\Delta\varepsilon|$. Larger S means more sensitivity to environmental permittivity. In the following exploration, we choose layer A as the perturbation and set the initial permittivity $\varepsilon_a = 4$. Then we replace the permittivity ε_a to ε'_a ranging from 3.95 to 4.05, corresponding to the slight change $\pm 1.25\%$ of the initial environmental permittivity. Thus the dielectric constant changing degree $\Delta\varepsilon = \varepsilon'_a - \varepsilon_a$ and the Rabi splitting difference $\Delta E^R = E^R(\varepsilon'_a) - E^R(\varepsilon_a)$. Rabi splitting energy and the sensitivity within and without topological structure are given as E^R_{topo}, S_{topo} and E^R_{notopo}, S_{notopo},

respectively. The size of the silver nanoantenna is fixed with $r = 6.5\,\text{nm}$, $a = 21.45\,\text{nm}$, and $d = 5\,\text{nm}$.

Above all, a tiny small-bulk defect is taken into consideration. As shown in Fig. 3(a), the permittivity's changing only appears in the selected pink-marked cuboid area with $63 \times 63 \times 157\,\text{nm}^3$ semi-surrounding the nanoantenna within the half layer A. The same small-bulk dielectric is also set up in the nontopological module. The comparison of Rabi splitting energy E^R and sensitivity S between topological and nontopological systems is given in Fig. 3(c). For the small-bulk defect, the topological Rabi splitting energy E^R_{topo} is larger than nontopological E^R_{notopo} due to the inhibition of the cavity loss caused by topological protection. In comparison, the topological sensitivity S_{topo} is smaller than the nontopological sensitivity S_{notopo}, showing the stability of the strong coupling regime in the topological structure. When $\varepsilon'_a \geqslant 4.04$, E^R_{notopo} drops down to 0, and S_{notopo} jumps up to 423–529 meV because of the destruction of the strong coupling regime. Meanwhile, the topological structure still provides small S_{topo} and stable E^R_{topo}. It shows that, even if the defect is strong enough to break the strong coupling regime in nontopological situations, the topological structures can still protect strong coupling systems.

Then we consider the situation of a single-layer defect, as shown in Fig. 3(b) that only the middle half layer A semi-surrounding the nanoantenna gets involved in the change of permittivity ε'_a, which is pink-marked. The same dielectric is set up in the nontopological module. The Rabi splitting and sensitivity results are shown in Fig. 3(d), similar to small-bulk defects. E^R_{topo} is larger than E^R_{notopo} because of less cavity loss, and S_{topo} is smaller than S_{notopo}, leading to the robustness of strong coupling with topology. Moreover, when $\varepsilon'_a \geqslant 4.045$, the nontopological system cannot remain the strong coupling and E^R_{notopo} is down to 0 with $S_{\text{notopo}} > 400\,\text{meV}$. However, the topological structure still protects the strong coupling. Rabi splitting E^R_{topo} changes very little compared to that of the initial permittivity $\varepsilon_a = 4$, and sensitivity S_{topo} is also tiny, showing that strong coupling is immune to defects under topological protection.

We also consider the impurities that the permittivity of all layers A fluctuates around 4, i.e., all layers A with $\varepsilon_a = \varepsilon'_a$. In the control group of nontopological structures, we also set $\varepsilon_a = \varepsilon'_a$. Figures 3(e) and 3(f) give E^R and S for the nanoantenna with $r = 6.5\,\text{nm}$, $a = 21.45\,\text{nm}$, $d = 5\,\text{nm}$, and $r = 7\,\text{nm}$, $a = 22.58\,\text{nm}$, $d = 5\,\text{nm}$, respectively, as the function of ε_a. It is easy to find that E^R_{topo} is always larger than E^R_{notopo} because of smaller κ. Though there is no significant difference between S_{topo} and S_{notopo} among the neighborhood of $\varepsilon_a = 4$ in the strong coupling regime, S_{notopo} quickly jumps to the magnitude of $10^2\,\text{meV}$ due to the break of strong coupling when ε_a is away from 4 and E^R_{notopo} is down to 0. However, E^R_{topo} is always stable and S_{topo} keeps a small value, meaning that topology protects strong coupling from impurities. Also, by comparing the results of nanoantenna with $r = 6.5\,\text{nm}$ and $r = 7\,\text{nm}$, one can find that the topological protection is more evident in larger cavities because it is more challenging to keep the strong coupling from impurities.

The defects and impurities we discuss above belong to the deviation-kind disorder caused by the deviation of materials in the fabrication. However, another kind of disorder, the random-kind disorder, should also be considered, conforming to the practical reality, caused by the natural fluctuations of materials. Here we set ε_a as the random permittivity of all layers A by Gaussian distribution with $(\mu_{\text{Gauss}}, \sigma^2_{\text{Gauss}}) = (4, 5\%)$. By comparing $N = 15$ groups of random permittivity ε_a, we give the Rabi splitting E^R shown in Fig. 3(g). It is easy to find that all values of Rabi splitting with random permittivity are stable, with the average value $E^R_{\text{ave}} = 27.82\,\text{meV}$ and coefficient of variation $c_v = 3.32\%$. Therefore, we show that strong coupling is also immune to the random-kind disorder under topological protection.

It is worth stressing that the detuning $\Delta = \omega_c - \omega_a$ between the emitter and resonant nanoantenna should be considered for Rabi splitting E^R because varying ε_a or ε'_a affects the resonant cavity mode. Here we take the example of nanoantenna with $r = 6.5\,\text{nm}$, $a = 21.45\,\text{nm}$, and $d = 5\,\text{nm}$. For the small-bulk defect, the detuning Δ_{topo} of the topological system is -0.25–$0.25\,\text{meV}$ with $\varepsilon'_a = 3.95$–4.05, which is much smaller than $\Delta_{\text{notopo}} = -7.61$–$7.36\,\text{meV}$. Similar results appear for the single-layer defect that $\Delta_{\text{topo}} = -3.81$–$3.56\,\text{meV}$ is smaller than $\Delta_{\text{notopo}} = -7.61$–$7.61\,\text{meV}$. Thus topological protection also suppresses detuning for defects. However, for impurities, topology seems to lose the ability to reduce detuning, such that $\Delta_{\text{topo}} = -8.97$–$9.10\,\text{meV}$ is a little larger than $\Delta_{\text{notopo}} = -8.06$–$7.86\,\text{meV}$.

Overall, by combining the changes in Rabi splitting with and without topological protection under the defects and impurities, one can find that the Rabi splitting under topological protection is always larger and more stable than that of nontopological systems. The change of strong coupling caused by external environmental perturbations under topological protection is less than that of the nontopological situation; even if this environmental change destroys the nontopological strong coupling regime, the strong coupling under topological protection can still be maintained. Therefore, it can be proved that the topological optical states can effectively protect the strong coupling against the influence of environmental defects and impurities.

V. DISCUSSION ON THE ROLE OF TOPOLOGICAL PROTECTION

One may doubt that the protection of strong coupling is due to the presence of the photonic band-gap structure rather than topological properties. Here we show that the nontopological defect photonic structures as environment cannot protect strong coupling. A nontopological photonic structure with defect mode is constructed, consisting of layers A and B with ten periods, shown in Figs. 4(a) and 4(b). The middle layer A′ changes its thickness to $d'_a = 218.81\,\text{nm}$ to obtain the defect mode at $\lambda = 722.4\,\text{nm}$ in the photonic band gap, while the other parameters are the same as in the topological case. The nanoantenna is placed parallel to the interface between the middle layer B and the defect layer A′, and

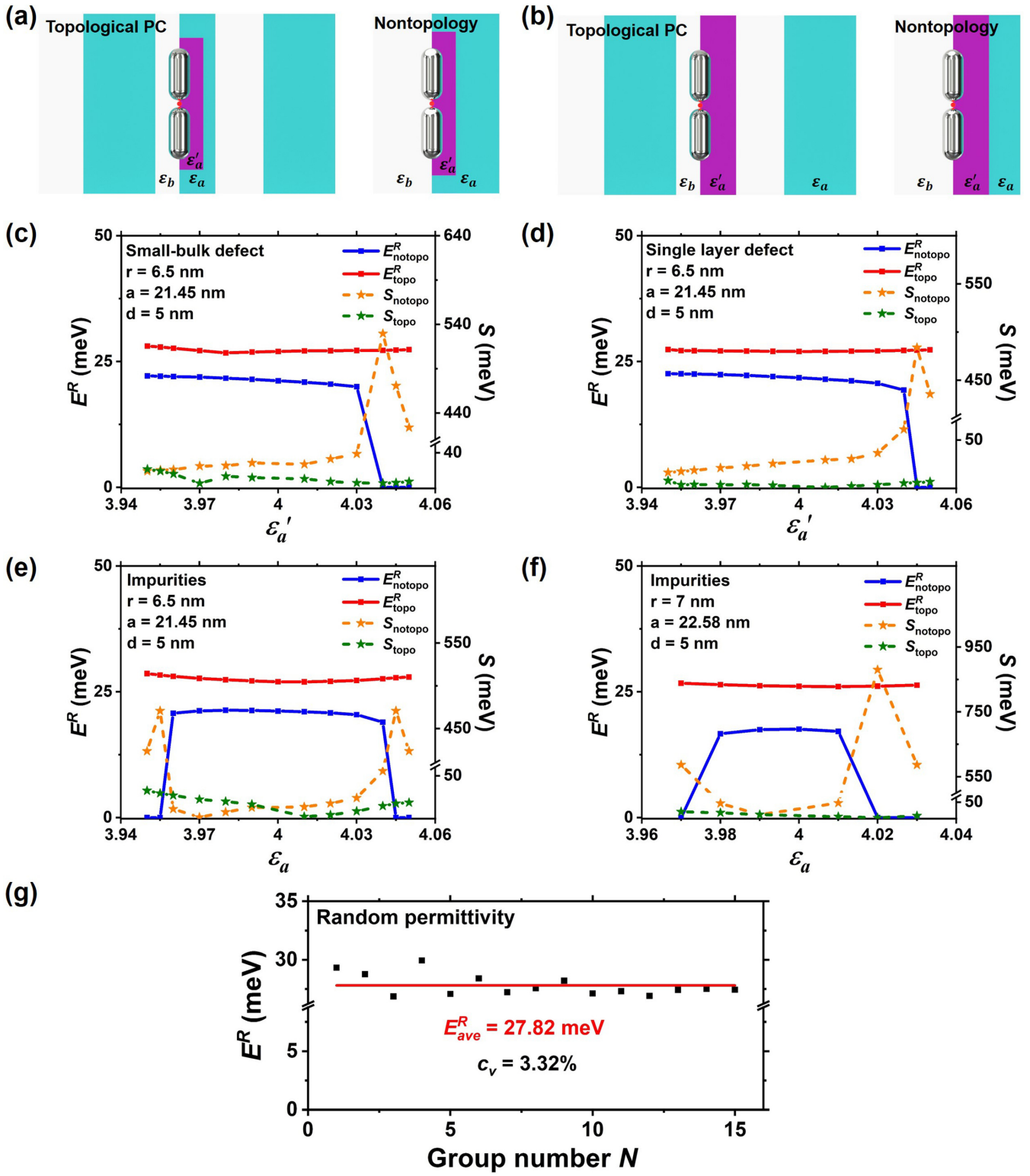

FIG. 3. The behavior of strong coupling systems disturbed by different defects or impurities with and without topological structure. Schematic diagrams of (a) small-bulk defects and (b) single-layer defects for topological and nontopological systems. The defects are marked by pink areas with varying permittivity ε_a' while other dielectric layers keep $\varepsilon_a = 4$ and $\varepsilon_b = 1$. The comparison of Rabi splitting energy E^R and sensitivity S between topological and nontopological systems for (c) small-bulk defects, (d) single-layer defects, (e) impurities with nanoantenna $r = 6.5\,\text{nm}$, $a = 21.45\,\text{nm}$, $d = 5\,\text{nm}$, and (f) impurities with nanoantenna $r = 7\,\text{nm}$, $a = 22.58\,\text{nm}$, $d = 5\,\text{nm}$. (g) Rabi splitting protected by topological structure against Gaussian-distribution random permittivity ε_a with $(\mu_{\text{Gauss}}, \sigma^2_{\text{Gauss}}) = (4, 5\%)$.

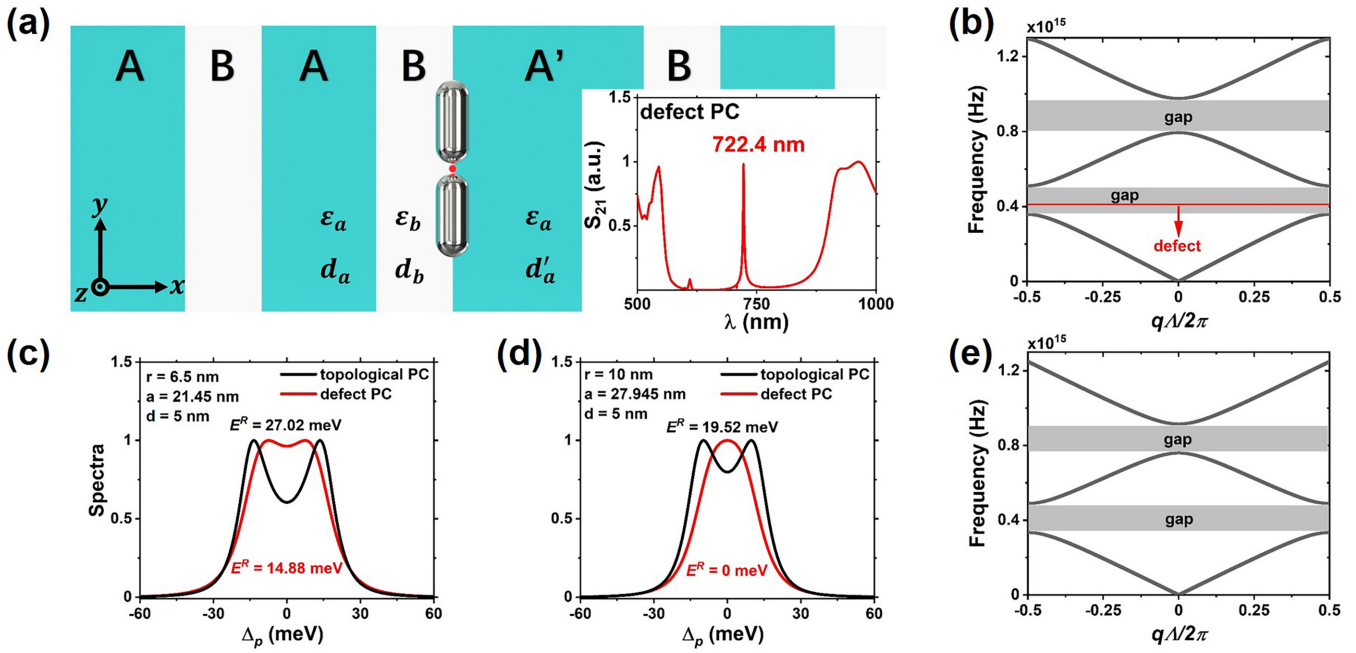

FIG. 4. The comparison of Rabi splitting in topological and nontopological photonic crystal structures. (a) Schematic diagram of the 1D nontopological photonic structure wrapping a resonant silver nanoantenna and a single emitter, with a defect layer A′ bringing the defect guide mode at 722.4 nm. (b) The band-gap structure of 1D trivial PC with defect mode. Rabi splitting with topological and nontopological photonic crystal structures with the parameters of nanoantenna (c) $r = 6.5$ nm, $a = 21.45$ nm, $d = 5$ nm, and (d) $r = 10$ nm, $a = 27.945$ nm, $d = 5$ nm, as a function of Δ_p. The defect layer A′ changes its thickness from d_a to $d'_a = 218.81$ nm. (e) The band-gap structure of 1D trivial PC without any guide mode.

divided into two equal parts. Here we take the nanoantenna with $r = 6.5$ nm, $a = 24.5$ nm, and $d = 5$ nm as an example. Note that the discussed cavity mode is still provided by the silver nanoantenna. The nanocavity loss $\kappa = 41.55$ meV of the defect nontopological case is much larger than that of the topological PC case [Fig. 2(a)], and even larger than that of the non-PC case [Fig. 2(a)], which should be caused by its localized defect mode. The spontaneous emission rate $\gamma = 1.80$ meV of the defect nontopological case gets slightly smaller than those of the non-PC and topological PC cases [Fig. 2(a)]. The coupling coefficient $g = 16.48$ meV of the defect nontopological case is almost identical to non-PC and topological PC cases [Fig. 2(a)]. Based on these parameters, as shown in Fig. 4(c), the Rabi splitting of the defect nontopological case is $E^R = 14.88$ meV, smaller than $E^R_{\text{topo}} = 27.02$ meV of the topological PC. Moreover, when the nanoantenna gets larger, like $r = 10$ nm, $a = 27.945$ nm, and $d = 5$ nm, the Rabi splitting of the defect nontopological case is down to 0 meV [Fig. 4(d)], while the Rabi splitting under topological protection remains. Thus the nontopological defect photonic structures as environment cannot protect strong coupling.

The photonic crystal structure environment without any guide mode in the working band gap is also considered [Fig. 4(e)], which is designed as $d_a = d_b = 120$ nm, $n_a = 2$, and $n_b = 1$. When the nanoantenna is with $r = 6.5$ nm, $a = 21.45$ nm, and $d = 5$ nm, the parameters of the CQED system are $\kappa = 37.82$ meV, $\gamma = 3.32$ meV, and $g = 16.48$ meV, leading to Rabi splitting $E^R = 19.14$ meV, which is close to $E^R_{\text{notopo}} = 21.18$ meV of the non-PC case, and smaller than $E^R_{\text{topo}} = 27.02$ meV of the topological case [Fig. 2(d)]. It is noted that $\kappa = 37.82$ meV of the trivial PC case is close to $\kappa = 35.25$ meV of the non-PC case, which means the band-gap structure of the trivial PC cannot directly affect the cavity loss in our systems. Therefore, the strong photon-exciton coupling regime is protected due to topology, not the optical cavity or photonic band-gap structure.

Finally, we briefly address the possibility of the experimental realization of our proposal. The nanoantennas can be fabricated by state-of-the-art nanotechnology [13,52,71], and the construction of topological photonic crystals has also been well established [30]. For example, the 1D grating heterostructures are practical for generating the edge state of the 1D topological PC structure [60]. The quantum emitter is considered an essential part of a strong coupling system. Several emitters can be unitized for experiments, such as classical atoms [72–74], Rydberg atoms [75], quantum dots [13,76,77], and molecular aggregates [16,17,78], providing dipole moment μ with a wide range from 0.07 to 40 enm, which is enough for strong coupling. The enormous challenge is integrating all these elements above into a high-precision nanostructure. In the past, metal nanoparticles have been placed to create nanoscale gap structures, which benefited strong coupling research [14,79,80]. One can apply similar nanotechnology in more complex hybrid structures such as topologically protected plasmonic strong coupling systems. Therefore, according to all the technologies above, it is possible to realize our proposal of topologically protected strong coupling systems experimentally in the future.

VI. CONCLUSION

In conclusion, we explored that the strong photon-exciton coupling caused by a silver nanoantenna and a single emitter can be protected in the 1D topological photonic structure environment. The response of strong coupling under topological protection differs from the nontopological situation. Topology protection results in an evident reduction in metal cavity losses, bringing greater Rabi splitting. As a type of quantum effect, the strong coupling regime can be effectively protected by topology, thereby making it immune to defects or impurities, even if this environmental change is enough to destroy the strong coupling regime in the absence of topology. Our results show that topological protection can reduce the threshold of achieving strong coupling and keep the strong coupling regime more stable, which is of great help for on-chip-integrated quantum devices, single-photon sources, and quantum information processing.

ACKNOWLEDGMENTS

We thank Ying Gu for the helpful discussions. This work was supported by National Key Research and Development Program of China (Grant No. 2022YFA1404804) and the National Natural Science Foundation of China (Grants No. 62325501 and No. 62135001).

[1] H. J. Kimble, The quantum internet, Nature (London) **453**, 1023 (2008).
[2] T. Pellizzari, S. A. Gardiner, J. I. Cirac, and P. Zoller, Decoherence, continuous observation, and quantum computing: A cavity QED model, Phys. Rev. Lett. **75**, 3788 (1995).
[3] C. Monroe, Quantum information processing with atoms and photons, Nature (London) **416**, 238 (2002).
[4] R. Miller, T. E. Northup, K. M. Birnbaum, A. Boca, A. D. Boozer, and H. J. Kimble, Trapped atoms in cavity QED: Coupling quantized light and matter, J. Phys. B: At. Mol. Opt. Phys. **38**, S551 (2005).
[5] Z. Qian, L. Shan, X. Zhang, Q. Liu, Y. Ma, Q. Gong, and Y. Gu, Spontaneous emission in micro-Or nanophotonic structures, PhotoniX **2**, 21 (2021).
[6] X. Duan, F. Zhang, Z. Qian, H. Hao, L. Shan, Q. Gong, and Y. Gu, Accumulation and directionality of large spontaneous emission enabled by epsilon-near-zero film, Opt. Express **27**, 7426 (2019).
[7] Z. Jacob and V. M. Shalaev, Plasmonics goes quantum, Science **334**, 463 (2011).
[8] M. S. Tame, K. McEnery, Ş. Özdemir, J. Lee, S. A. Maier, and M. Kim, Quantum plasmonics, Nat. Phys. **9**, 329 (2013).
[9] O. Benson, Assembly of hybrid photonic architectures from nanophotonic constituents, Nature (London) **480**, 193 (2011).
[10] H. J. Kimble, Strong interactions of single atoms and photons in cavity QED, Phys. Scr. **1998**, 127 (1998).
[11] F. Brennecke, T. Donner, S. Ritter, T. Bourdel, M. Köhl, and T. Esslinger, Cavity QED with a Bose-Einstein condensate, Nature (London) **450**, 268 (2007).
[12] H. Deng, H. Haug, and Y. Yamamoto, Exciton-polariton Bose-Einstein condensation, Rev. Mod. Phys. **82**, 1489 (2010).
[13] S. Savasta, R. Saija, A. Ridolfo, O. Di Stefano, P. Denti, and F. Borghese, Nanopolaritons: Vacuum Rabi splitting with a single quantum dot in the center of a dimer nanoantenna, ACS Nano **4**, 6369 (2010).
[14] R. Chikkaraddy, B. De Nijs, F. Benz, S. J. Barrow, O. A. Scherman, E. Rosta, A. Demetriadou, P. Fox, O. Hess, and J. J. Baumberg, Single-molecule strong coupling at room temperature in plasmonic nanocavities, Nature (London) **535**, 127 (2016).
[15] A. E. Schlather, N. Large, A. S. Urban, P. Nordlander, and N. J. Halas, Near-field mediated plexcitonic coupling and giant Rabi splitting in individual metallic dimers, Nano Lett. **13**, 3281 (2013).
[16] J. Bellessa, C. Bonnand, J. C. Plenet, and J. Mugnier, Strong coupling between surface plasmons and excitons in an organic semiconductor, Phys. Rev. Lett. **93**, 036404 (2004).
[17] G. Zengin, M. Wersäll, S. Nilsson, T. J. Antosiewicz, M. Käll, and T. Shegai, Realizing strong light-matter interactions between single-nanoparticle plasmons and molecular excitons at ambient conditions, Phys. Rev. Lett. **114**, 157401 (2015).
[18] T. K. Hakala, J. J. Toppari, A. Kuzyk, M. Pettersson, H. Tikkanen, H. Kunttu, and P. Törmä, Vacuum Rabi splitting and strong-coupling dynamics for surface-Plasmon polaritons and rhodamine 6G molecules, Phys. Rev. Lett. **103**, 053602 (2009).
[19] D. E. Gómez, K. C. Vernon, P. Mulvaney, and T. J. Davis, Surface plasmon mediated strong exciton-photon coupling in semiconductor nanocrystals, Nano Lett. **10**, 274 (2010).
[20] K. M. Birnbaum, A. Boca, R. Miller, A. D. Boozer, T. E. Northup, and H. J. Kimble, Photon blockade in an optical cavity with one trapped atom, Nature (London) **436**, 87 (2005).
[21] T. Peyronel, O. Firstenberg, Q.-Y. Liang, S. Hofferberth, A. V. Gorshkov, T. Pohl, M. D. Lukin, and V. Vuletić, Quantum nonlinear optics with single photons enabled by strongly interacting atoms, Nature (London) **488**, 57 (2012).
[22] H. Hao, L. Shan, Q. Zhang, X.-C. Yu, Q. Gong, and Y. Gu, Quantum state transfer with seamless frequency-connection through diamond optomechanical cavity, Adv. Quantum Technol. **4**, 2000127 (2021).
[23] T. Tiecke, J. D. Thompson, N. P. de Leon, L. Liu, V. Vuletić, and M. D. Lukin, Nanophotonic quantum phase switch with a single atom, Nature (London) **508**, 241 (2014).
[24] Q. Zhang, H. Hao, J. Ren, F. Zhang, Q. Gong, and Y. Gu, A quantum phase gate capable of effectively collecting photons based on a gap plasmon structure, Nanoscale **12**, 10082 (2020).
[25] Z. Qian, J. Ren, F. Zhang, X. Duan, Q. Gong, and Y. Gu, Nanoscale quantum plasmon sensing based on strong photon-exciton coupling, Nanotechnology **31**, 125001 (2020).
[26] N. Kongsuwan, X. Xiong, P. Bai, J.-B. You, C. E. Png, L. Wu, and O. Hess, Quantum plasmonic immunoassay sensing, Nano Lett. **19**, 5853 (2019).
[27] L. Lu, J. D. Joannopoulos, and M. Soljačić, Topological photonics, Nat. Photon. **8**, 821 (2014).

[28] L. Lu, J. D. Joannopoulos, and M. Soljačić, Topological states in photonic systems, Nat. Phys. **12**, 626 (2016).
[29] A. B. Khanikaev and G. Shvets, Two-dimensional topological photonics, Nat. Photon. **11**, 763 (2017).
[30] T. Ozawa, H. M. Price, A. Amo, N. Goldman, M. Hafezi, L. Lu, M. C. Rechtsman, D. Schuster, J. Simon, O. Zilberberg, and I. Carusotto, Topological photonics, Rev. Mod. Phys. **91**, 015006 (2019).
[31] L.-H. Wu and X. Hu, Scheme for achieving a topological photonic crystal by using dielectric material, Phys. Rev. Lett. **114**, 223901 (2015).
[32] S. Barik, A. Karasahin, C. Flower, T. Cai, H. Miyake, W. DeGottardi, M. Hafezi, and E. Waks, A topological quantum optics interface, Science **359**, 666 (2018).
[33] M. Xiao, Z. Q. Zhang, and C. T. Chan, Surface impedance and bulk band geometric phases in one-dimensional systems, Phys. Rev. X **4**, 021017 (2014).
[34] W. S. Gao, M. Xiao, C. T. Chan, and W. Y. Tam, Determination of zak phase by reflection phase in 1D photonic crystals, Opt. Lett. **40**, 5259 (2015).
[35] Y. Ota, F. Liu, R. Katsumi, K. Watanabe, K. Wakabayashi, Y. Arakawa, and S. Iwamoto, Photonic crystal nanocavity based on a topological corner state, Optica **6**, 786 (2019).
[36] Y. Zhao, F. Liang, J. Han, X. Wang, D. Zhao, and B.-Z. Wang, Tunable topological edge and corner states in an all-dielectric photonic crystal, Opt. Express **30**, 40515 (2022).
[37] C. W. Hsu, B. Zhen, A. D. Stone, J. D. Joannopoulos, and M. Soljačić, Bound states in the continuum, Nat. Rev. Mater. **1**, 16048 (2016).
[38] F. Wang, X. Yin, Z. Zhang, Z. Chen, H. Wang, P. Li, Y. Hu, X. Zhou, and C. Peng, Fundamentals and applications of topological polarization singularities, Front. Phys. **10**, 862962 (2022).
[39] W. P. Su, J. R. Schrieffer, and A. J. Heeger, Solitons in polyacetylene, Phys. Rev. Lett. **42**, 1698 (1979).
[40] A. Blanco-Redondo, I. Andonegui, M. J. Collins, G. Harari, Y. Lumer, M. C. Rechtsman, B. J. Eggleton, and M. Segev, Topological optical waveguiding in silicon and the transition between topological and trivial defect states, Phys. Rev. Lett. **116**, 163901 (2016).
[41] S. Xia, D. Kaltsas, D. Song, I. Komis, J. Xu, A. Szameit, H. Buljan, K. G. Makris, and Z. Chen, Nonlinear tuning of pt symmetry and non-hermitian topological states, Science **372**, 72 (2021).
[42] M. Hafezi, S. Mittal, J. Fan, A. Migdall, and J. Taylor, Imaging topological edge states in silicon photonics, Nat. Photon. **7**, 1001 (2013).
[43] S. Mittal, V. V. Orre, G. Zhu, M. A. Gorlach, A. Poddubny, and M. Hafezi, Photonic quadrupole topological phases, Nat. Photon. **13**, 692 (2019).
[44] X. Yin, J. Jin, M. Soljačić, C. Peng, and B. Zhen, Observation of topologically enabled unidirectional guided resonances, Nature (London) **580**, 467 (2020).
[45] Z. Chen, X. Yin, J. Jin, Z. Zheng, Z. Zhang, F. Wang, L. He, B. Zhen, and C. Peng, Observation of miniaturized bound states in the continuum with ultra-high quality factors, Sci. Bull. **67**, 359 (2022).
[46] S. Mittal, E. A. Goldschmidt, and M. Hafezi, A topological source of quantum light, Nature (London) **561**, 502 (2018).
[47] P. St.-Jean, V. Goblot, E. Galopin, A. Lemaître, T. Ozawa, L. Le Gratiet, I. Sagnes, J. Bloch, and A. Amo, Lasing in topological edge states of a one-dimensional lattice, Nat. Photon. **11**, 651 (2017).
[48] X.-T. He, E.-T. Liang, J.-J. Yuan, H.-Y. Qiu, X.-D. Chen, F.-L. Zhao, and J.-W. Dong, A silicon-on-insulator slab for topological valley transport, Nat. Commun. **10**, 872 (2019).
[49] Z. Qian, Z. Li, H. Hao, L. Shan, Q. Zhang, J. Dong, Q. Gong, and Y. Gu, Absorption reduction of large purcell enhancement enabled by topological state-led mode coupling, Phys. Rev. Lett. **126**, 023901 (2021).
[50] A. Blanco-Redondo, B. Bell, D. Oren, B. J. Eggleton, and M. Segev, Topological protection of biphoton states, Science **362**, 568 (2018).
[51] T. Dai, Y. Ao, J. Bao, J. Mao, Y. Chi, Z. Fu, Y. You, X. Chen, C. Zhai, B. Tang *et al.*, Topologically protected quantum entanglement emitters, Nat. Photon. **16**, 248 (2022).
[52] A. Kinkhabwala, Z. Yu, S. Fan, Y. Avlasevich, K. Müllen, and W. Moerner, Large single-molecule fluorescence enhancements produced by a bowtie nanoantenna, Nat. Photon. **3**, 654 (2009).
[53] J.-W. Liaw, Analysis of a bowtie nanoantenna for the enhancement of spontaneous emission, IEEE J. Sel. Top. Quantum Electron. **14**, 1441 (2008).
[54] D. E. Chang, A. S. Sørensen, P. R. Hemmer, and M. D. Lukin, Quantum optics with surface plasmons, Phys. Rev. Lett. **97**, 053002 (2006).
[55] J. Ren, Y. Gu, D. Zhao, F. Zhang, T. Zhang, and Q. Gong, Evanescent-vacuum-enhanced photon-exciton coupling and fluorescence collection, Phys. Rev. Lett. **118**, 073604 (2017).
[56] J. Ren, H. Hao, Z. Qian, X. Duan, F. Zhang, T. Zhang, Q. Gong, and Y. Gu, High-dielectric constant enhanced photon 2013;exciton coupling in an evanescent vacuum, J. Opt. Soc. Am. B **35**, 1475 (2018).
[57] D. Smirnova, D. Leykam, Y. Chong, and Y. Kivshar, Nonlinear topological photonics, Appl. Phys. Rev. **7**, 021306 (2020).
[58] Y. Ota, K. Takata, T. Ozawa, A. Amo, Z. Jia, B. Kante, M. Notomi, Y. Arakawa, and S. Iwamoto, Active topological photonics, Nanophotonics **9**, 547 (2020).
[59] C. Poli, M. Bellec, U. Kuhl, F. Mortessagne, and H. Schomerus, Selective enhancement of topologically induced interface states in a dielectric resonator chain, Nat. Commun. **6**, 6710 (2015).
[60] C. Li, X. Hu, W. Gao, Y. Ao, S. Chu, H. Yang, and Q. Gong, Thermo-optical tunable ultracompact chip-integrated 1D Photonic topological insulator, Adv. Opt. Mater. **6**, 1701071 (2018).
[61] E. Jaynes and F. Cummings, Comparison of quantum and semiclassical radiation theories with application to the beam maser, Proc. IEEE **51**, 89 (1963).
[62] C. Guerlin, E. Brion, T. Esslinger, and K. Mølmer, Cavity quantum electrodynamics with a Rydberg-blocked atomic ensemble, Phys. Rev. A **82**, 053832 (2010).
[63] H. J. Carmichael, *Statistical Methods in Quantum Optics* (Springer-Verlag, Berlin, 2008).
[64] P. Meystre and M. Sargent, III, *Elements of Quantum Optics* (Springer, Berlin, 1990).
[65] M. O. Scully, M. S. Zubairy *et al.*, *Quantum Optics* (Cambridge University Press, Cambridge, England, 1997).
[66] H. Lian, Y. Gu, J. Ren, F. Zhang, L. Wang, and Q. Gong, Efficient single photon emission and collection based on excitation of gap surface plasmons, Phys. Rev. Lett. **114**, 193002 (2015).
[67] X. Shan, I. Diez-Perez, L. Wang, P. Wiktor, Y. Gu, L. Zhang, W. Wang, J. Lu, S. Wang, Q. Gong *et al.*, Imaging the

electrocatalytic activity of single nanoparticles, Nat. Nanotechnol. **7**, 668 (2012).

[68] J. Johansson, P. Nation, and F. Nori, Qutip: An open-source python framework for the dynamics of open quantum systems, Comput. Phys. Commun. **183**, 1760 (2012).

[69] P. B. Johnson and R. W. Christy, Optical constants of the noble metals, Phys. Rev. B **6**, 4370 (1972).

[70] J. Noh, W. A. Benalcazar, S. Huang, M. J. Collins, K. P. Chen, T. L. Hughes, and M. C. Rechtsman, Topological protection of photonic mid-gap defect modes, Nat. Photon. **12**, 408 (2018).

[71] T. Taminiau, F. Stefani, F. B. Segerink, and N. Van Hulst, Optical antennas direct single-molecule emission, Nat. Photon. **2**, 234 (2008).

[72] K. Patil, R. Pawar, and P. Talap, Self-aggregation of methylene blue in aqueous medium and aqueous solutions of bu4nbr and urea, Phys. Chem. Chem. Phys. **2**, 4313 (2000).

[73] D. A. Steck, Cesium d line data, revision 1.6 (accessed: 21 november 2019), http://steck.us//alkalidata.

[74] D. A. Steck, Rubidium 87 d line data, revision 2.2.1 (accessed: 9 july 2021), http://steck.us//alkalidata.

[75] S.-S. Zhang, H. Cheng, P.-P. Xin, H.-M. Wang, Z.-S. Xu, and H.-P. Liu, A sensitive detection of high Rydberg atom with large dipole moment, Chin. Phys. B **27**, 074207 (2018).

[76] D. Gammon and D. G. Steel, Optical studies of single quantum dots, Phys. Today **55**, 36 (2002).

[77] A. Ridolfo, O. Di Stefano, N. Fina, R. Saija, and S. Savasta, Quantum plasmonics with quantum dot-metal nanoparticle molecules: Influence of the fano effect on photon statistics, Phys. Rev. Lett. **105**, 263601 (2010).

[78] W. Wang, P. Vasa, R. Pomraenke, R. Vogelgesang, A. De Sio, E. Sommer, M. Maiuri, C. Manzoni, G. Cerullo, and C. Lienau, Interplay between strong coupling and radiative damping of excitons and surface plasmon polaritons in hybrid nanostructures, ACS Nano **8**, 1056 (2014).

[79] X. Chen, Y.-H. Chen, J. Qin, D. Zhao, B. Ding, R. J. Blaikie, and M. Qiu, Mode modification of plasmonic gap resonances induced by strong coupling with molecular excitons, Nano Lett. **17**, 3246 (2017).

[80] R. Liu, Z.-K. Zhou, Y.-C. Yu, T. Zhang, H. Wang, G. Liu, Y. Wei, H. Chen, and X.-H. Wang, Strong light-matter interactions in single open plasmonic nanocavities at the quantum optics limit, Phys. Rev. Lett. **118**, 237401 (2017).